Adsorption of mercury ions from synthetic and real wastewater aqueous solution by functionalized multi-walled carbon nanotube with both amino and thiolated groups

Mojtaba Hadavifar[a], Nader Bahramifar[b*], Habibollah Younesi[a], Qin Li[c]

[a] Department of Environmental Science, Faculty of Natural Resources, Tarbiat Modares University, P.O. Box 46414-356, Noor, Iran

[b] Department of chemistry, Payam Noor University (PNU), POBOX 1939-3697, Tehran, Iran

[c] Department of Environmental Engineering & Queensland Micro- and Nanotechnology Centre, Griffith University, Nathan Campus, P.O. Box 4111, Brisbane, Australia

Abstract

The functionalization of multi-walled carbon nanotubes (MWCNTs) was using with ethylenediamine and cyanuric chloride and sodium 2-mercaptoethanol as efficient ways to introduce amine and thiol functional groups onto the nanotube sidewalls. The synthesized amino and thiolated MWCNTs were characterized by Fourier transform infrared spectroscopy (FT-IR), thermogravimetric analysis (TGA), X-ray photoelectron spectroscopy (XPS) and scanning electron microscope (SEM). A series of batch adsorption experiments were conducted to study the effect of pH, dose, metal concentration and temperature on Hg(II) uptake by the functionalized, MWCNTs. The isotherm data were analyzed for possible agreement with the Langmuir than Freundlich models, while the equilibrium data were fitted better by Langmuir model. The pseudo-first-order and pseudo-second-order rate equations were tested on kinetic

* Corresponding author: Tel: +98 151325896, Fax: +98 1513258960, E-mail address: nbahramifar@yahoo.com (N. Bahramifar)

data and an adsorption followed the pseudo-second-order rate kinetics. Based on the thermodynamic data of ΔH^o, ΔS^o and ΔG^o obtained, it can be concluded that the Hg(II) ion adsorption on the functionalized MWCNTs is exothermic, spontaneous and the mechanism of physical adsorption. In a fixed-bed column adsorption, the effects of bed height, flow rate and initial ion concentration on the breakthrough curve were investigated, on which the predictions were found to be satisfactory both by the Yan and Thomas models. Lastly, we found out the as-synthesized MWCNTs with good efficiency for Hg(II) removal from real wastewater.

Keywords: Functionalized MWCNTs, mercury adsorption, thiol functional group, thermodynamic parameters, kinetics

1. Introduction

Mercury is a highly toxic and accumulative metal and its compounds, especially methyl mercury, are neurotoxins which cause blockage of the enzyme sites and interfere in protein synthesis. The fate of inorganic, mercury ions in nature is its turning into methyl mercury due to the aerobic action of microorganisms [1]. The main sources of mercury ions in aquatic ecosystems are divergent, chloralkali wastewater, oil refineries, power generation plants, paper and pulp manufacturing**,** rubber processing and fertilizers industries [2]. Various methods have been used for removing heavy metals from aqueous environment such as reverse osmosis, chemical precipitation, ion exchange, coagulation and adsorption [3]. Many carbon-based nanoparticles (CNTs) have been developed to remove heavy metals from aqueous media [2,4–6]. They are promising material for numerous applications due to their unique electrical, mechanical, thermal, optical and chemical properties. In addition, CNTs are proven to be superior adsorbents for

several divalent metal ions in water, because of their capability to establish (π-π) electrostatic interactions as well as for their large surface areas [7–9]. Therefore, they have received considerable attention for usage in analytical chemistry and environmental remediation [10]. Multi-walled carbon nanotubes (MWCNTs) were the first observed CNTs involving of up to several tens of graphite shells [11]. The sorption capability of MWCNTs is related mainly to the functional groups attached on its surface [12]. Generations of functional groups on the surface carbon nanotubes improves the reactivity and provides active sites for further chemical modifications [13]. Many researchers have developed amino [10,14] and thiol [15–18] functionalization on carbon-based adsorbents and CNTs in order to increase the adsorption capacity and removal efficiency of heavy metals and organic compounds. Among these functional groups, the thiols have an excellent binding ability to some metals such as silver, mercury, copper, nickel and zinc [18,19]. So far, integrated existence of amino and thiol functional groups on the surface of CNTs has not been reported and nor as having been applied as adsorbent for heavy metals.

In the present study, we prepared new integrated amino and thiol functional groups on the MWCNT surface for removal of mercury ions from an aqueous solution. The As-synthesized products were characterized by Fourier transform infrared spectroscopy (FT-IR), thermogravimetric analysis (TGA), X-ray photoelectron spectroscopy (XPS) and scanning electron microscope (SEM). Adsorption of mercury ions from aqueous solution was carried out in batch and continuous systems. The factors affecting the adsorption of Hg(II) onto the functionalized MWCNT**s** (pH, ion concentration, feed flow rate, temperature, adsorbent dosage and bed height) were investigated. The data thus obtained were fitted with the Freundlich and Langmuir isotherm models in the batch system and with Yan and Thomas models in the

continuous mode. The thermodynamic properties, including enthalpy, entropy and Gibbs free energy, of the functionalized MWCNTs were determined from the experimental data. Desorption and recovery of Hg(II) was also studied for the subsequent recycling. Finally, the capability of thiolated MWCNTs for the removal of Hg(II) ion from chloralkali wastewater was investigated.

2. Experimental

2.1. Materials and reagents

MWCNTs were obtained from Timesnano Chinese Academy of Sciences Company. The purity was more than 95%, outside diameter (OD) 20-30 nm, inside diameter (ID) 5-10 nm, length 10-30 μm, specific surface area (SSA) more than 110 m^2/g, density 0.28 g/cm^3 and electrical conductivity (EC) more than 100 s/cm. 1,5-diphenylthiocarbazone (Dithizone), hydrochloric acid (37% HCl), methanol, ethanol, tetrahydrofuran (THF), $HgCl_2$, ethylenediamine (EDA), concentrated H_2SO_4 and HNO_3 acids, 2,4,6-trichloro-1,3,5-triazine (cyanuric chloride), n,n-di-isopropylethylamine (DIPEA), n,n-dicyclohexylcarbodiimide (DCC) and cetyltrimethylammonium bromide (CTAB) obtained from Merck (Germany). The sodium 2-mercaptoethanol was prepared controlled conditions by reacting metallic sodium with 2-mercaptoethanol (from Merck).

2.2. Synthesis process

2.2.1. MWCNTs-COOH

Raw-MWCNT (5 g) was treated with 10% HCl for 3 h and 15 min sonication (180 W, 53 kHz,) to remove impurities such as metal particles, residual catalysts and amorphous carbons in the stage of synthesis (**Fig. 1-a**). Then the sample was filtered and washed many successive times

with distilled water to reach a neutral pH. In order to chemically oxidize and prepare the carboxylated MWCNTs (MWCNTs-COOH), the sample was suspended in 400 ml 10 N H_2SO_4 and HNO_3 (3:1 by volume) and refluxed at 175 ^oC for 18 h in Teflon flask, then filtered and washed with hot distilled water until the pH was neutral, and dried at 180 ˚C for 1 h (**Fig. 1- b)** [20] .

2.2.2. MWCNTs-EDA

For synthesis of the amino modified MWCNTs-EDA, 4 g of MWCNTs-COOH was placed in a 150 ml EDA solution while stirring at 100 rpm and temperature of 25 ^oC, then 5 g of DCC was added and refluxed for 48 h at 78 ^oC. The product was passed through a filter paper and washed with ethanol and dried at 80 ^oC for 8 h (**Fig. 1- c**) [21].

2.2.3. MWCNTs-triazine

In order to blend the triazine into the MWCNTs-EDA, 8.86 g of cyanuric chloride was dissolved in 480 ml of THF and then 11.5 ml of DIPEA was added and stirred at 0 ^oC for 3 h under argon atmosphere. Then 3 g of MWCNTs-EDA was added to this mixture and stirred at 0 ^oC for 48 h under argon atmosphere; during this reaction time the chlorine atom in cyanuric chloride was substituted by the amine group in EDA and the released HCl was trapped by DIPEA. Then the sample was filtered and washed with dried THF repeatedly to remove the excess cyanuric chloride and dried at 80 ^oC for 8 h (**Fig. 1- d**) [22]. The prepared product denoted MWCNTs-triazine.

2.2.4. MWCNTs-SH

The aromatic triazine ring in the MWCNTs-triazine has two chlorine atoms which can be substituted by thiol functional groups. With that in mind, 25 ml of sodium 2-mercaptoethanol was mixed with 30 ml methanol, then 2 g of MWCNTs-triazine was added to the mixture and refluxed at 50 ^{o}C for 12 h, stirring at low speed. The sample was filtered and rinsed with methanol and dried at 80 ^{o}C for 3 h (**Fig. 1- e**). The thiolated product was denoted as MWCNTs-SH.

2.3. Characterization of adsorbents

The FT-IR spectra were recorded (Shimadzu FT-IR 8400s spectrometer, Japan) in the range of 500-4000 cm^{-1} and TGA was also carried out (Rheometric Scientific, STA 1500, USA) from an ambient temperature to 700 ^{o}C in nitrogen atmosphere using a heating rate of 10 ^{o}C/min. The XPS was used to analyze the functionalized MWCNTs by a twin anode XR3E2 x-ray source system (8025-BesTec, Germany). The surface morphologies of the MWCNTs, MWCNTs-COOH, MWCNTs-EDA, MWCNTs-triazine and MWCNTs-SH were characterized using SEM images (Hitachi S-4160, Japan, 1996) at accelerating voltage of 20 kV.

2.4. Batch adsorption experiments

Batch adsorption experiments were conducted in 250 ml conical flasks containing 100 ml of Hg(II) ion solution stirring at 200 rpm and room temperature of 25 ^{o}C. The equilibrium study was carried out by sampling at different time intervals and equilibrium was assumed at 60 min. The samples were filtered by a 0.42 µm pore size paper filter. A stock solution of 1000 mg/l of Hg(II) was prepared by an exact amount of $HgCl_2$ in deionized water (EC <0.05 µS/m), diluting daily to the desired concentration. The Hg(II) concentrations in solution was measured by

spectrophotometric method [23]. The removal efficiency of Hg(II) ion was calculated by the following equation:

$$R = \frac{C_o - C_t}{C_o} \times 100 \quad (1)$$

where R is the removal efficiency of the Hg(II), C_0 the initial concentration and C_t the final concentration Hg(II) in mg/l at t time. The adsorption capacity of the adsorbent at equilibrium was calculated by the following equation:

$$q_e = \frac{(C_o - C_o)V}{W} \quad (2)$$

where q_e is the equilibrium adsorption capacity of the adsorbent in mg/g, C_0 the initial concentration in mg/l and C_e the equilibrium concentration of Hg(II) in mg/l, V the volume in L of Hg(II) solution and W the weight in g of the adsorbent. The analyses were done in duplicate with the average values reported.

2.4.1. Effect of the adsorbent dose

In the batch experiments, the effects of the dose of the adsorbent (100, 200, 400 and 600 mg/l) on adsorption of Hg(II) at 10 mg/l were studied. The pH of the working solution was adjusted to 7 by 0.1 M NaOH. For all experiments, fresh diluted ion solutions were prepared daily.

2.4.2. Effect of the solution pH

The effect of a different pH of the initial solution on adsorption was investigated in pH range of 2 to 8 by adding 0.1 M HNO_3 and 0.1 M NaOH solution. The working volume was 100 ml, the adsorbent dose and the ion concentration was 400 and 10 mg/l, respectively. The samples

contained 250 ml conical flasks were stirred at 200 rpm to reach equilibrium. The concentration of the remaining Hg(II) ion was measured after filtration at designed intervals.

2.4.3. Effect of temperature

The effect of temperature (15, 25, 35 and 45 ^{o}C) on Hg(II) adsorption was studied with 40 mg of MWCNTs-SH in 100 ml of 40 mg/l metal ion solution at pH 6.

2.5. Adsorption isotherms

A study to determine the relationship between the Hg(II) ion adsorbed on MWCNTs-SH and those remaining in the aqueous phase was conducted. All experiments were carried out with the various initial Hg(II) concentrations (5, 10, 20, 40, 80 and 100 mg/l) in conditions of: fixed amount of absorbent 40 mg per 100 ml solution, constant pH 6, room temperature (25 ^{o}C) and 200 rpm agitation speed. Contact time was 60 min for all equilibrium conditions. The isotherm data were correlated with the Freundlich and Langmuir models. The Langmuir isotherm is based on a monolayer sorption of metal ion on the surface of the adsorbent and is described by the following equation [24]:

$$q_e = \frac{q_m b C_e}{1 + b C_e} \qquad (3)$$

where, q_e is the adsorption capacity of the adsorbent in mg/g and C_e the concentration of metal ion in mg/l at equilibrium. The q_m is the maximum adsorption capacity of the metal monolayer in mg/g, and b the constant that refers to the bonding energy of adsorption in l/mg. The Freundlich isotherm model is considered to be appropriate for describing both multilayer sorption and sorption on heterogeneous surfaces. The Freundlich model can be expressed by the following equation [22]:

$$q_e = K_f C_e^{1/n} \quad (4)$$

where, q_e is the equilibrium adsorption capacity of the adsorbent in mg/g, C_e the liquid phase concentration in mg/l at equilibrium, K_f the constant related to the adsorption capacity of the adsorbent and n the empirical constant depicting the intensity of adsorption which varies with the heterogeneity of the adsorbent. The greater is the value of n the better its adsorption capacity. The nonlinear regression analysis was carried out with SigmaPlot software (SigmaPlot 10.0, USA) in order to predict both the K_f and the n parameters.

2.6. Kinetic studies

The kinetic studies were carried out using 40 mg of MWCNTs-SH in 100 ml of different concentrations (5, 10, 20, 40, 80 and 100 mg/l) of Hg(II) metal ion solutions at pH 6. In order to describe the kinetic process between aqueous and solid phase, the pseudo-first-order rate was used for surface adsorption of Hg(II) ion on MWCNTs-SH. This model is presented by Lagergren as follows [25]:

$$Log(q_e - q_t) = Log q_e - \frac{k_1}{2.303} t \quad (5)$$

The pseudo-second-order rate equation presented by Ho to describe the kinetic adsorption of divalent metal ion onto an absorbent is expressed as follows [26]:

$$\frac{t}{q_t} = \frac{1}{k_2 q_e^2} + \frac{t}{q_e} \quad (6)$$

where q_e and q_t are the amount of adsorbed metal ion in mg/g on the adsorbent, at equilibrium and time t, respectively, while k_1 in min^{-1} and k_2 $gmg^{-1}min^{-1}$ are the rate constants of first- and second-order adsorption, respectively [27,28].

2.7. Adsorption thermodynamics

The adsorption studies were conducted at different temperatures (15, 25, 35, and 45 ^{o}C) with 40 mg/l of Hg(II) ion concentration for investigating the thermodynamic parameters by calculating the free energy of Gibbs (ΔG^{o}) according to the following equation [29]:

$$LnK_d = \frac{\Delta S^o}{R} - \frac{\Delta H^o}{RT} \quad (7)$$

where the values of ΔH^{o} (change in enthalpy in J mol^{-1}) and ΔS^{o} (change in entropy in J mol^{-1}K^{-1}) are obtained from the slope and intercept of *Ln* k_d vs. *1/T* plot, *T* is the temperature in K and *R* the universal gas constant (8.314 Jmol^{-1} K^{-1}). The distribution coefficient (k_d) is calculated from the initial and the equilibrium concentrations (C_0 and C_e) of the metal ion [7]:

$$k_d = \frac{C_o - C_e}{C_e} \times \frac{V}{W} \quad (8)$$

where, *V* is the working volume in L and *W* the adsorbent mass in g. The ΔG^{o} is the change in Gibbs free energy in J mol^{-1}, calculated according to the following equation [29]:

$$\Delta G^o = \Delta H^o - T\Delta S^o \quad (9)$$

2.8. Fixed bed column adsorption studies

The adsorption capability of MWCNTs-SH for removal of Hg(II) ion in solution was studied using a fixed-bed glass column in the form of a lab scale apparatus with an inside diameter of 5 mm. Fig 2 demonstrates the schematic of lab scale apparatus of continuous adsorption. As the figure shows, the prepared solution containing Hg(II) ion was passed through the column using a peristaltic pump (pump drive 5101, Heidolph, Germany) in upward mode. The experiments were carried out at various bed heights (7, 14 and 21 mm) of MWCNTs-SH, at various influent flow rates (1, 1.5 and 2 ml/min) and various initial Hg(II) ion concentrations (20, 40 and 60 mg/l), at

pH 6 and room temperature. These conditions were chosen according to optimum conditions obtained in the batch studies. The effluent samples were collected at appropriate time intervals.

2.8.1. Fixed bed column data analysis and modeling

The effluent concentration trend versus the time profile gave the breakthrough curve. The breakthrough time, t_b, is considered to be when the metal concentration in the effluent (C_{eff}) reaches about 5% of the influent concentration (C_o), representing the still active column. The exhausting time, t_e, is assumed when the metal concentration in the effluent reaches 95% of the influent concentration. The area surrounded by the breakthrough curve represents the total metal ion mass adsorbed (q_{total}, mg) which is evaluated by the following equation:

$$q_{total} = \frac{QC_o}{1000}\int_{t=0}^{t=t_{total}} \left(1 - \frac{C_{eff}}{C_o}\right) dt \qquad (10)$$

where $(1\text{-}C_{eff}/C_0)$ is the concentration of metal ion absorbed (mg/l) and Q the flow rate (ml/min) that can be determined by Eq. (11).

$$Q = \frac{V_{eff}}{t_{total}} \qquad (11)$$

The total amount metal ion passed through the column (mg) can be obtained from the Eq. (12) and the total removed metal evaluated by dividing the metal mass absorbed (q_{total}) by the total amount of metal ion passed the column (m_{total}), as shown in Eq. (13):

$$m_{total} = \frac{C_o \times Q \times t_e}{1000} \qquad (12)$$

$$R = \frac{q_{total}}{m_{total}} \times 100 \qquad (13)$$

The equilibrium adsorption capacity, q_e (mg/g), and the equilibrium metal concentration, C_e (mg/l), can be obtained from the following equations, respectively:

$$q_e = \frac{q_{total}}{m} \tag{14}$$

$$C_e = \frac{m_{total} - q_{total}}{V_{eff}} \times 1000 \tag{15}$$

where m is the adsorbent mass (g). The mass transfer zone (MTZ) is the region of the bed where most of the adsorption occurs and moves up through the bed column in time to be evaluated by Eq. (16) [22]:

$$MTZ = L\frac{t_e - t_b}{t_e} \tag{16}$$

where L is the bed height (cm), t_b and t_e are the time (min) required to achieve the breakthrough point and the exhaust point, respectively.

Successful designing of the column adsorption needs to be able to predict the concentration-time breakthrough curve for the effluent. The maximum capability of an adsorbent is also required in the design. The Thomas model (Thomas, 1948) is used traditionally to achieve this purpose and expressed as follows [30]:

$$\frac{C_{eff}}{C_o} = \frac{1}{1 + \exp\left(\frac{k_T}{Q}\left(q_T M - C_o V\right)\right)} \tag{17}$$

where C_e (mg/l) is the metal ion concentration in effluent, C_0 the influent metal ion concentration in mg/l, k_T the Thomas rate constant in ml/min.mg, q_T the maximum solid-phase concentration of solution in mg/g, M the mass of the adsorbent in g, V the throughput volume in ml and Q the influent flow rate in ml/min. The Yan model is an empirical equation overcoming the deficiencies in the Thomas model, especially its serious deficit in predicting the effluent

concentration at time zero. It was found to define the breakthrough curve better in a fixed bed column. This equation is expressed as follows [31]:

$$\frac{C_{eff}}{C_o} = 1 - \frac{1}{\left(\frac{QC_o t}{q_Y M}\right)^a} \quad (18)$$

where q_Y is the maximum adsorption capacity (mg/g) of adsorbent estimated by the Yan model and a the constant coefficient.

2.9. Batch desorption study

Any prepared adsorbent must be renewable in practice, or synthetized MWCNTs-SH should also be reusable several times in adsorption-desorption cycles. Reusability of MWCNTs-SH was determined in five adsorption-desorption cycles. To optimize the type and concentration of the acid, the experiments were carried out with different concentrations (0.1, 0.3 and 0.5 M) of HCl, H_2SO_4 and HNO_3. Then the acid with more efficiency in desorption of loaded Hg(II) ion on the MWCNTs-SH was selected. After each cycle the regenerated adsorbent was washed twice by distilled water and centrifuged to remove the remainder ion, from the adsorbent. The metal recovery was calculated by the following Eq. (19) [32]:

$$\text{metal recovery} = \frac{\text{Amount of metal ions desorbed}}{\text{Amount of metal ions adsorbed}} \times 100 \quad (19)$$

2.10. Real wastewater study

In order to survey capability of the prepared adsorbents for removal of Hg(II) from actual wastewater, some batch experiments were conducted on chloralkali wastewater. The wastewater sample was taken from effluent sewage of wastewater treatment plan of petrochemical

chloralkali unit of Mahshahr, Iran. An sufficient amount of nitric acid was added to sample to prevent adsorption of mercury ions by the plastic walls of container. The sample was held in a cooled flask with ice bag and transported to laboratory for study. After adjusting the pH to 6, 100 ml of sample was placed in four 250 ml conical flask and 20 mg of each adsorbent (MWCNTs, MWCNTs-COOH, MWCNTs-EDA and MWCNTs-SH) was added and stirred for 60 min. After than the Hg(II) content of all samples was determined by an inductively coupled plasma mass (ICP-Ms) method (PerkinElmer, Optima 7300 DV, USA).

3. Results and discussion

3.1. Characterization of adsorbents

The FT-IR peaks in the range of 500-4000 cm^{-1}, related to pristine and functionalized MWCNTs, are recorded in Fig**. 3-a**. The H_2SO_4-HNO_3 treatment introduces the carboxyl group on the MWCNTs during oxidation. The presence of peaks at ≈3438 and ≈1726 cm^{-1} are related to the stretching vibrations of ν(OH) and ν(C=O) of the carboxyl groups (COOH), respectively, [10] which become stronger and deeper in the MWCNTs-COOH rather than the MWCNTs. Symmetric and asymmetric methylene stretching bands at ≈2850 and ≈2920 cm^{-1}, respectively, are observed to be present in the MWCNTs and MWCNTs-COOH. It is assumed that defective sites on the sidewall of MWCNTs contain these groups [20]. The peak at ≈1097 cm^{-1} is assigned to the ν(C–O) stretching vibration [10] which becomes sharper in the MWCNTs-COOH compared to the MWCNTs and disappears after amine functionalization. A peak at ≈3378 cm^{-1} overlapping with the stretching vibration of ν(-OH) in the MWCNTs-EDA is due to the -NH_2 stretching of the amine group [10,33] that confirms the successful engulfing of the EDA to carboxyl groups. In the MWCNTs-triazine the three successive peaks from ≈800 to ≈1300 cm^{-1}

are due to incorporation of the melamine-based molecule to EDA tails of the MWCNTs-EDA. The C–Cl and C–N bond stretchings at ≈763 and ≈1180 cm^{-1}, respectively, are detectable [34,35]. Those at ≈1531 and ≈1492 cm^{-1} and at ≈1178 cm^{-1} were assigned to C=N and C–N groups in the triazine ring, respectively [36]. The new weak peak at ≈2668 cm^{-1} in MWCNTs-SH may be attributed to the S–H bond vibration.

It should be mentioned that the S–S or C=S bond that maybe appeared in thiol functionalization were observed [15], but hardly detectable in the FT-IR spectra. Therefore, the XPS was used to confirm the thiolation of the MWCNTs. In **Fig. 3-b**, a series of XPS survey spectra for the MWCNTs-EDA and MWCNTs-SH are shown. The XPS data show the peaks corresponding to C, O and N1s and S2p. The peaks were calibrated with a value of C1s peak at 284.5 eV [16]. The C1s peaks are derived from graphitic and aromatic groups, like phenolic, hydroxyl or ether groups, and carbonyl and carboxylic or ester groups. The O1s peak at 533.0 eV includes oxygen in carbonyl groups, hydroxyl or ethers, anhydride, lactone, or carboxylic acids. The N1s peaks were from nitrogen atoms in the functional groups of NH–, N–O, –CON or $CONH_2$ at 400.0-401.5 eV in MWCNTs-EDA [37]. With increase in nitrogen atoms in the MWCNTs-SH, related to the triazine ring, the nitrogen peak there becomes broader (397.0 - 401.5 eV) compared to that in the MWCNTs-EDA and they split due to the different chemical bonds of –O–C–N or –O–C=N groups. A S2p peak appeared in the MWCNTs-SH spectrum at 163.7 eV, which is due to the $–CH_2–SH$ bond [38,39], confirming the successful synthesis of the MWCNTs-SH.

Fig. 3-c shows the TGA curves. The samples were heated at a rate of 10 ^oC/min in a nitrogen atmosphere to 700 ^oC. The pristine MWCNTs did not have a noticeable weight loss until the temperature reached 500 ^oC, due to the pretreatment of pristine MWCNTs for removal of impurities with 10% HCl, but afterwards they decomposed sharply from 500 to 700 ^oC. The loss

of weight of MWCNTs-EDA occurred at lower temperatures compared with pristine MWCNTs because most of the organic functional moieties on the MWCNTs-EDA are thermally unstable [10]. The most weight loss was achieved at 250 to 300 ^{o}C (1.4%) and the total thermal decomposition from 200 to 500 ^{o}C was 4.33% attributed to dislocations of carbon materials, covalently bonded EDA and oxygenated groups on the surface of MWCNTs-EDA. In the same manner the most weight loss of MWCNTs-SH occurred at 250 to 300 ^{o}C (3.38%) and the total mass loss of 8.7% happened in the temperature range of 200 to 500 ^{o}C. The greater weight loss of MWCNTs-SH indicates the presence of amine and thiol functional groups on the surface of MWCNTs. A comparison of SEM images of MWCNTs, MWCNTs-COOH, MWCNTs-EDA, MWCNTs-triazine and MWCNTs-SH are shown in Fig. **3-d**. All samples were sputtered with gold before imaging. As shown in Fig. **3-d**, no changes in morphology has occurred in all samples where the nanotubes do not appear to be damaged or shortened during oxidation at severe and harsh experimental conditions. The images show that most of the tubes are in parallel arrangement to one another after treatments. This may be due to strong intertubular electrostatic interactions between surface functional groups. On the other hands, the hydrophobic surface of MWCNTs leading to repulsion among tubes, resulted in a random arrangement of nanotubes [40]. Furthermore, it is noticeable that there are more open ends (bright patches) on the MWCNTs-COOH compared to raw MWCNTs, suggesting that nanotubes become more active at the ends and sidewalls [41]. Created defect sites and covalently attached functional groups, especially in amine modified cases (MWCNTs-EDA and MWCNTs-triazine), can cause a reduction in electric conductivity of nanotubes, which may be the reason for the blurring shape of the images and reduction of the contrast and resolution [42].

3.2. Adsorption of Hg(II) metal ion in batch system

3.2.1. Effect of adsorbent dose

The batch experiments were carried out to compare the efficiency of different adsorbents for Hg(II) ion removal, a comparison of which for five adsorbents at different doses is depicted in **Fig. 4**. According to these data, the MWCNTs-SH can be considered to be a more effective adsorbent than the others. Furthermore, increasing the adsorbent dose increases the ion removal percentage due to a boost in the available fresh sites on the absorbent. The tendency of Hg(II) to bind to the thiol functional group has been proved [43]. The Hg(II), Cd(II) and Pb(II) are metal ions with low-charge density, considered soft acids that form strong covalent bonds to soft bases such as sulfur [44]. Although carboxylated and amino modified MWCNTs have been used for removal of divalent metals [10,21], no other metal forms as strong a covalent bond with a thiol functional group as mercury ion does (200 kJ mol^{-1}). It is well-known that the ligands containing aromatic backbones with two additional thiol arms can bind the Hg in a linear S-Hg-S arrangement [45]. These types of ligands are effective at removing mercury ions from aqueous solutions. Furthermore, in our synthesized MWCNTs-SH, two thiol functional groups have been attached to alkyl chains that provide the high flexibility to achieve the linear S-Hg-S arrangement (**Fig. 1-e**).

3.2.2. Effect of solution pH

The pH of the solution plays an important role on the adsorption of ion metals. In order to determine the effect of pH on the Hg(II) ion removal by MWCNT-SH, some experiments were carried out with different pH values while the other parameters were constant. As is shown in

Fig. 5, the Hg(II) removal increases from 9.8% to 92% with increase in the pH from 2 to 8, respectively. The solution pH has a different effect on adsorption depending on the type of adsorbent and functional groups. The removal of mercury ions by powdered activated carbon revealed that the removal efficiency decreases with an increasing pH [3]. The reaction mechanism of the SH functional group and mercury ions species are formulated as equations (20) and (21) [43].

$$2R\text{-}SH + Hg^{2+} \rightarrow R\text{-}S\text{-}Hg\text{-}S\text{-}R + 2H^{+} \quad (20)$$

$$R\text{-}SH + HgCl^{+} \rightarrow R\text{-}S\text{-}HgCl + H^{+} \quad (21)$$

It can be discerned from these reactions that increasing the OH^- lead to consumption of H^+ in the solution, allowing the reactions to proceed properly. In contrast, increasing the H^+ in the solution causes competition between hydrogen and metal ion for active binding sites, whereby the removal percentage decreases. Furthermore, the more preferable species of metal ion at higher pH are the $Hg(OH)_3^-$, $Hg(OH)_2$ and $Hg(OH)^+$ compound forms, which have smaller effective size and higher mobility than Hg(II) [18,46,47].

3.3. Adsorption isotherms

Adsorption isotherms contain certain constant parameters expressing the surface properties and affinity of the adsorbent, making it possible to evaluate the adsorption capacity of the adsorbent for metal ion. The nonlinear Langmuir and Freundlich adsorption isotherms of the Hg(II) ion (evaluated at the adsorbent dose of 400 mg/l and 25 ^oC temperature) are shown in **Fig. 6**. The parameters of Langmuir and Freundlich isotherms (b, q_m, n and k_f) and the nonlinear regression correlation coefficients (R^2) are given in **Table 1**. A sharp initial slope in both isotherms indicate that the efficiency of the adsorbent is high in low Hg(II) concentrations and it decreases with an

increase in the metal ion concentration due to the saturation of active sites on the adsorbent surface. As shown in **Table 1**, the correlation coefficients indicate that the adsorption tended to be fitted better by the Langmuir (R^2=0.945) than the Freundlich model (R^2=0.926). Thus, the adsorption can be described by the Langmuir Isotherm and the metal ion adsorption occurs on an homogeneous surface by monolayer sorption without interaction between the adsorbed ion, whereas the Freundlich model expresses multilayer adsorption with a heterogeneous energetic distribution of active sites with interactions between the adsorbed ion [24]. The maximum adsorption capacity (q_m) obtained with Langmuir was 84.66 mg/g, which is higher than some recently thiolated CNTs such as 65.52 mg/g with MPTS-CNT/Fe_3O_4 [18] and 72.8 µg/g with S-MWCNTs [46] for Hg(II) removal.

3.4. Adsorption thermodynamics

The effect of temperature on the adsorption of Hg(II) ion onto MWCNTs-SH has been illustrated by a linear plot of lnk_d versus 1/T in **Fig. 7**, and the estimated thermodynamic parameters and correlation coefficients calculated from Eqs. (7-9) are summarized in **Table 2**. Under the steady-state reaction conditions, the Gibbs free energy (ΔG^o) ranges from -3.18 to -4.59 kJ mol^{-1}, and the ΔH^o and ΔS^o are -18.12 kJ mol^{-1} and -0.047 J mol^{-1} K^{-1}, respectively, indicating that lower temperatures favor spontaneous reaction for Hg(II) adsorption by MWCNTs-SH. The negative values of ΔH^o with a decreasing trend of k_d with increasing temperature revealed that the adsorption of Hg(II) onto the MWCNTs-SH is exothermic. The negative values of ΔG^o indicate that the adsorption of Hg(II) onto MWCNTs-SH is spontaneous. However, the $\Delta G°$ values increase with increasing temperature, indicating that the adsorption is more efficient at lower temperatures. As to whether the adsorption of Hg(II) onto MWCNTs-SH is chemisorption or

physisorption, it is noted that the covalent bonding of mercury ion with thiol functional groups releases 200 kJ mol^{-1}, and that the change in ΔG° for physisorption happens at between (-20 and 0 kJ mol^{-1}), while the physisorption and chemisorption together occur within the range of (-20 to -80 kJ mol^{-1}), chemisorption being within the range of (-80 to -400 kJ mol^{-1}) [48]. The obtained ΔG° values indicate that interactions between Hg(II) and MWCNTs-SH can be considered as physisorption mechanism. On the other hand, it is accepted that physical adsorption involves an enthalpy change in the range of (2 to 21 kJ mol^{-1}), while the heat for chemisorption generally falls into a range of (80-200 kJ mol^{-1}) [49]. The low value of ΔS° implies that no noticeable change in entropy occurred during the Hg(II) adsorption and the negative value of ΔS° indicates a tendency to lower disorder at the solid-solution interface during adsorption. In addition, it also reflects no occurrence of ion replacement reactions, because the increased entropy of the system could have happened due to release of the ion from the solid surface to the solution [10]. On the other hand, in adsorption processes release of the water molecules produced by ion exchange reactions between the metal ion and the surface functional groups of the adsorbent can increase ΔS° [50].

3.5. Desorption

The desorption efficiency of MWCNTs-SH was evaluated by HCl, H_2SO_4 and HNO_3 acid treatment. The 0.5 M HCl was more effective than other concentrations as well as other acid types. The adsorbent was reused in five successive adsorption-desorption cycles as can be seen in **Fig. 8**, indicating a loss in the adsorption capacity of 7.2% for Hg(II) compared to the initial cycle, revealing a good regeneration capacity of the adsorbent. This is different from what Pillay *et al*. [46] have reported whereas no desorption was observed in their prepared S-MWCNTs due

to strong bonding of the Hg(II) to sulfur functional groups on the adsorbent surfaceand even acid washing was unable to release the mercury ions. . As mentioned before, the MWCNTs-SH prepared in this study contains two free thiol chains that can bind to Hg(II) in a linear arrangement, depending strongly on the pH of the solution, whereby desorption can be achieved at low pH. The good desorption rate also confirms that the Hg(II) adsorption is physisorption.

3.6. Adsorption kinetics

Typical kinetic experimental curves for adsorption of Hg(II) on the MWCNTs-SH in different ion concentrations showed that ion adsorption increases sharply during a short contact time (5 min) and slows down gradually to reach equilibrium (Figure not shown). In order to describe the kinetics for Hg(II) ion adsorption onto the MWCNTs-SH, the pseudo-first-order and pseudo-second-order kinetics are applied (Figures not shown). The parameters of the kinetic models and the regression correlation coefficients (R^2) are listed in **Table 3**. The R^2 values clearly indicate the validity of the pseudo-second-order versus pseudo-first-order kinetics which is not fitted logically. As seen in Table 3, when the initial ion concentration increases from 5 to 100 mg/l, the pseudo-second-order constants (k_2) decrease from 2.05 to 0.0025 g/mg min. This indicates that the available active sites on the MWCNTs-SH are saturated rapidly by Hg(II) ion, furthermore suggesting the possibility of the formation of a monolayer coverage of Hg(II) onto the adsorbent [2].

3.7. Adsorption of Hg(II) in fixed bed column

3.7.1. Effect of bed height

Fixed-bed column experiments were conducted using filled columns with MWCNTs-SH for three different bed heights (of 7, 14 and 21 mm) at a constant flow rate of 1.5 ml/min and an influent Hg(II) concentration of 40 mg/l. The breakthrough curves at different bed heights are shown in **Fig. 9-a** and the breakthrough analysis summarized in **Table 4**. At a constant flow rate, with increase in the bed height from 7 to 14 mm, the removal percentage increases from 42.46 to 57% due to more active sites in the column. Also, because the MTZ needs more time to reach the column end, the metal ion have more time to be in contact with the absorbent, but in bed height of 21 mm no noticeable removal occurs (53.97%), because it takes longer for the column to reach exhaustion time, more solution can pass through the column, so the removal obtained is less than that for the bed height of 14 mm. According to Table 4, both the greater q_e (91.37 mg/g) and the removal percentage denote results for the bed height of 14 mm rather than those of 7 and 21 mm. Thus the optimum bed height can be considered as 14 mm.

3.7.2. Effect of flow rate

The breakthrough curves for Hg(II) at various flow rates (of 1, 1.5 and 2 ml/min) through a 7 mm bed height column and an influent concentration of 40 mg/l are shown in **Fig. 9-b** and the breakthrough parameters presented in **Table 4**. These results reveal that with increasing the flow rate from 1 to 2 ml/min, the breakthrough curve shows shorter time to reach the column exhaustion. The breakthrough analysis shows that at the flow rates of 1, 1.5 and 2 ml/min, the q_e values are 105.65, 76.42 and 71.47 mg/g and MTZ values 4.41, 6.35 and 6.79 mm, respectively. By increasing the flow rate, the metal ion do not have enough time to bind to the absorbent as they would have passed the column before reaching equilibrium, so the column active life is significantly reduced [22], and a higher q_e obtained at flow rate of 1 ml/min. At the lower flow

rate (1 m l/min) the MTZ is located in the lower section of the column (4.41 mm), so the metal ion have enough time to bind to the adsorbent along the column, but at higher flow rates the MTZ shifts to the end of the column, which can diminish the time needed for binding the metal ion.

3.7.3. Effect of influent metal ion concentration

The effect of the influent metal ion concentration on the adsorption of the Hg(II) was investigated by using it in various concentrations (of 20, 40 and 60 mg/l) at a constant bed height of 7 mm and flow rate of 1 ml/min. The results are presented in **Fig**. **9-c** and **Table 4**. According to the figure, with increase in the initial ion concentration from 20 to 60 mg/l, the column exhaustion occurs faster due to an enhanced dispersion of metal ion along the column, besides this can have an effect on the MTZ length. As the breakthrough analysis shows in Table 4, the MTZ values obtained for concentrations of 20, 40 and 60 mg/l are 5.46, 4.41 and 4.13 mm, respectively. Increasing the initial ion concentration creates a driving force to diffuse the metal ion from the liquid phase into the surface of the adsorbent, hence the MTZ is shortened. However a higher q_e value is obtained with concentration of 40 mg/l (105.65 mg/g), but increasing the initial ion concentration further lead to concluding with a larger removal percentage. Thus for concentrations of 20, 40 and 60 mg/l, the removal obtained is 55.34, 64.03 and 69.30%, respectively. This trend is due to the decrease in the total passed volume of metal solution through the column with the increase in the influent metal ion concentration, until the column reaches to exhaustion time.

3.8. Fixed bed column modeling

The Thomas and Yan models were used for fitting the experimental data in order to determine the rate constant, maximum adsorption capacity and to predict the breakthrough curve for dynamic adsorption of Hg(II). The breakthrough curves, predicted by the Yan and Thomas models at different bed height, flow rate and various initial concentrations for Hg(II), are shown in **Fig. 9(a-c)**. All the parameters of the Thomas and Yan models for Hg(II) removal in columns for various conditions are presented in **Table 4**. As these parameters show, the obtained non-linear regression correlation coefficients (R^2) from the Yan model (ranging from 0.957 to 0.999) compared with those from the Thomas model (ranging from 0.978 to 0.996) are slightly higher, except for two cases (see Table 4). From this table, it can be seen that the obtained data were fitted better by the Yan than the Thomas model, but with no significant differences. On the other hand, the difference between the experimental adsorption capacity (q_e) of Hg(II) and the values predicted by the Thomas model (q_{Th}) are lower than those by the Yan model (q_Y). Thus the Thomas model is a more suitable kinetic model to describe the Hg(II) adsorption onto MWCNTs-SH in a fixed-bed column.

3.9. Chloralkali wastewater adsorption

In order to survey capability of the prepared adsorbents for removal of Hg(II) from actual wastewater, some batch experiments were conducted on chloralkali wastewater. Characteristics of chloralkali wastewater are summarized in **Table 5**. As the results show, chloralkali wastewater contains a high concentration of different ions, especially of total solids (TS) and EC, which can interfere with adsorption of Hg ion on the adsorbents. Thus the selectivity of the adsorbent is important. As the **Fig. 10** shows, the MWCNTs-SH is a good adsorbent with high

capability for adsorption of mercury ions (88.7%) from chloralkali wastewater in comparison with other modified MWCNTs.

4. Conclusions

Amino and thiol functional groups of MWCNTs were successfully prepared for the removal of mercury ions from synthetic chloralkali wastewater. The FT-IR, XPS, TGA and SEM analyses confirmed successful entailing the functional groups on the MWCNTs. The experiments revealed that the MWCNTs-SH has a good capability for Hg(II) ion removal from aqueous solution. At desired conditions of the batch system (pH 6 and adsorbent dose of 400 mg/l), the experimental maximum adsorption capacity of MWCNTs-SH for Hg(II) ion removal was achieved with 84.66 mg/g by Langmuir isotherm model. The equilibrium data were fitted by the Langmuir model (R^2 = 0.945) better than the Freundlich model (R^2 = 0.926). In the thermodynamic studies the values for ΔH^o and $\Delta S°$ were obtained as -18.12 kJ mol^{-1} and -0.047 $kJ^{-1}mol^{-1}K^{-1}$, respectively, indicating an exothermic and spontaneous nature of the adsorption. The physisorption mechanism of adsorption was confirmed by the negative values of $\Delta G°$ increased with increasing of temperature. The kinetic adsorption parameters showed that the overall adsorption can be described better by the pseudo-second-order than the pseudo-first-order kinetic model. The adsorption-desorption experiments showed a small loss in the adsorption capacity of 7.2% for Hg(II) after five cycles, indicating a good regeneration capacity of the adsorbent for treating wastewater containing mercury ions. In the continuous mode, effects on the breakthrough curve of bed height, flow rate and initial ion concentration were investigated, while the experimental adsorption capacity reached to 105.65 mg/g. The Thomas model predicted the maximum adsorption capacity better than the Yan model, but logically both models described the

breakthrough curves in all continuous modes of operation. Finally, we found out that our new synthesized MWCNTs-SH is a good adsorbent for mercury ions removal (by 88.7%) from chloralkali wastewater.

Acknowledgements

The authors appreciate the sponsorship of the Ministry of Science, Research and Technology of Iran and the financial support of the Tarbiat Modares University (TMU) by whose grant the present research was made possible. The authors wish also to thank Mrs. Haghdoust (Technical assistant of the Laboratory) for her assistance in laboratory works, and Ellen Vuosalo Tavakoli (University of Mazandaran) for final editing of the English text.

References

[1] A.M. Starvin, T.P. Rao, Removal and recovery of mercury(II) from hazardous wastes using 1-(2-thiazolylazo)-2-naphthol functionalized activated carbon as solid phase extractant., Journal of Hazardous Materials. 113 (2004) 75–9.

[2] M.F. Yardim, T. Budinova, E. Ekinci, N. Petrov, M. Razvigorova, V. Minkova, Removal of mercury (II) from aqueous solution by activated carbon obtained from furfural., Chemosphere. 52 (2003) 835–41.

[3] M. Zabihi, A. Ahmadpour, A. Asl, Removal of mercury from water by carbonaceous sorbents derived from walnut shell, Journal of Hazardous Materials. 167 (2009) 230–236.

[4] Y. Tian, B. Gao, V.L. Morales, L. Wu, Y. Wang, R. Muñoz-Carpena, et al., Methods of using carbon nanotubes as filter media to remove aqueous heavy metals, Chemical Engineering Journal. 210 (2012) 557–563.

[5] A.M. Starvin, T.P. Rao, Removal and recovery of mercury (II) from hazardous wastes using carbon as solid phase extractant, 113 (2004) 75–79.

[6] C.B. Wade, C. Thurman, W. Freas, J. Student, D. Matty, D.K. Mohanty, Preparation and characterization of high efficiency modified activated carbon for the capture of mercury from flue gas in coal-fired power plants, Fuel Processing Technology. 97 (2012) 107–117.

[7] O. Moradi, K. Zare, M. Monajjemi, M. Yari, H. Aghaie, The Studies of Equilibrium and Thermodynamic Adsorption of Pb(II), Cd(II) and Cu(II) Ions from Aqueous Solution onto SWCNTs and SWCNT–COOH Surfaces, Fullerenes, Nanotubes and Carbon Nanostructures. 18 (2010) 285–302.

[8] F. Taleshi, A. a Hosseini, Synthesis of uniform MgO/CNT nanorods by precipitation method, Journal of Nanostructure in Chemistry. 3 (2012) 4.

[9] M.M. Shokrieh, A. Saeedi, M. Chitsazzadeh, Mechanical properties of multi-walled carbon nanotube/polyester nanocomposites, Journal of Nanostructure in Chemistry. 3 (2013) 20.

[10] G.D. Vuković, A.D. Marinković, M. Čolić, M.Đ. Ristić, R. Aleksić, A.A. Perić-Grujić, et al., Removal of cadmium from aqueous solutions by oxidized and ethylenediamine-functionalized multi-walled carbon nanotubes, Chemical Engineering Journal. 157 (2010) 238–248.

[11] X. Ren, C. Chen, M. Nagatsu, X. Wang, Carbon nanotubes as adsorbents in environmental pollution management: A review, Chemical Engineering Journal. 170 (2011) 395–410.

[12] A.H. El-Sheikh, Y.S. Al-Degs, R.M. Al-As'ad, J. a. Sweileh, Effect of oxidation and geometrical dimensions of carbon nanotubes on Hg(II) sorption and preconcentration from real waters, Desalination. 270 (2011) 214–220.

[13] Y. Tao, Z. Lin, X.-M. Chen, X. Huang, M. Oyama, X. Wang, Functionalized multiwall carbon nanotubes combined with bis(2,2′-bipyridine)-5-amino-1,10-phenanthroline ruthenium(II) as an electrochemiluminescence sensor, Sensors and Actuators B: Chemical. 129 (2008) 758–763.

[14] G.D. Vuković, A.D. Marinković, S.D. Škapin, M.Đ. Ristić, R. Aleksić, A. a. Perić-Grujić, et al., Removal of lead from water by amino modified multi-walled carbon nanotubes, Chemical Engineering Journal. 173 (2011) 855–865.

[15] J.K. Lim, W.S. Yun, M. Yoon, S.K. Lee, C.H. Kim, K. Kim, et al., Selective thiolation of single-walled carbon nanotubes, Synthetic Metals. 139 (2003) 521–527.

[16] Y. Kim, T. Mitani, Surface thiolation of carbon nanotubes as supports : A promising route for the high dispersion of Pt nanoparticles for electrocatalysts, Journal of Catalysis. 238 (2006) 394–401.

[17] N.O. V Plank, R. Cheung, Thiolation of single-wall carbon nanotubes and their self-assembly, APPLIED PHYSICS LETTERS. 85 (2004) 3229–3231.

[18] C. Zhang, J. Sui, J. Li, Y. Tang, W. Cai, Efficient removal of heavy metal ions by thiol-functionalized superparamagnetic carbon nanotubes, Chemical Engineering Journal. 210 (2012) 45–52.

[19] D.A. Simoni, C. Airoldi, E.F.S. Vieira, I. De Quimica, U.E. De Campinas, C. Postal, Interaction of cations with SH-modified silica gel : thermochemical study through calorimetric titration and direct extent of reaction determination, 7 (1997) 2249–2252.

[20] B. Scheibe, E. Borowiak-palen, R.J. Kalenczuk, Oxidation and reduction of multiwalled carbon nanotubes — preparation and characterization, Materials Characterization. 61 (2010) 185–191.

[21] Z. Zang, Z. Hu, Z. Li, Q. He, X. Chang, Synthesis , characterization and application of ethylenediamine-modified multiwalled carbon nanotubes for selective solid-phase extraction and preconcentration of metal ions, 172 (2009) 958–963.

[22] A. Shahbazi, H. Younesi, A. Badiei, Functionalized SBA-15 mesoporous silica by melamine-based dendrimer amines for adsorptive characteristics of Pb(II), Cu(II) and Cd(II) heavy metal ions in batch and fixed bed column, Chemical Engineering Journal. 168 (2011) 505–518.

[23] H. Khan, M.J. Ahmed, M.I. Bhanger, A simple spectrophotometric determination of trace level mercury using 1,5-diphenylthiocarbazone solubilized in micelle., Analytical Sciences : the International Journal of the Japan Society for Analytical Chemistry. 21 (2005) 507–12.

[24] Y. Sağ, Y. Aktay, Application of equilibrium and mass transfer models to dynamic removal of Cr(VI) ions by Chitin in packed column reactor, Process Biochemistry. 36 (2001) 1187–1197.

[25] A. Heidari, H. Younesi, Z. Mehraban, Removal of Ni (II), Cd (II), and Pb (II) from a ternary aqueous solution by amino functionalized mesoporous and nano mesoporous silica, Chemical Engineering Journal. 153 (2009) 70–79.

[26] H. Qiu, L. Lv, B. Pan, Q. Zhang, W. Zhang, Q. Zhang, Critical review in adsorption kinetic models, Journal of Zhejiang University SCIENCE A. 10 (2009) 716–724.

[27] O. Moradi, K. Zare, Adsorption of Pb(II), Cd(II) and Cu(II) Ions in Aqueous Solution on SWCNTs and SWCNT –COOH Surfaces: Kinetics Studies, Fullerenes, Nanotubes and Carbon Nanostructures. 19 (2011) 628–652.

[28] D. Robati, Pseudo-second-order kinetic equations for modeling adsorption systems for removal of lead ions using multi-walled carbon nanotube, Journal of Nanostructure in Chemistry. 3 (2013) 55.

[29] A. a Farghali, M. Bahgat, W.M. a ElRouby, M.H. Khedr, Decoration of multi-walled carbon nanotubes (MWCNTs) with different ferrite nanoparticles and its use as an adsorbent, Journal of Nanostructure in Chemistry. 3 (2013) 50.

[30] G. Yan, T. Viraraghavan, Heavy metal removal in a biosorption column by immobilized M. rouxii biomass., Bioresource Technology. 78 (2001) 243–9.

[31] D. Pokhrel, T. Viraraghavan, Arsenic removal in an iron oxide-coated fungal biomass column: analysis of breakthrough curves., Bioresource Technology. 99 (2008) 2067–71.

[32] A. Shahbazi, H. Younesi, A. Badiei, Batch and fixed-bed column adsorption of Cu(II), Pb(II) and Cd(II) from aqueous solution onto functionalised SBA-15 mesoporous silica, The Canadian Journal of Chemical Engineering. 91 (2013) 739–750.

[33] G. Vuković, A. Marinković, M. Obradović, V. Radmilović, M. Čolić, R. Aleksić, et al., Synthesis, characterization and cytotoxicity of surface amino-functionalized water-dispersible multi-walled carbon nanotubes, Applied Surface Science. 255 (2009) 8067–8075.

[34] A. Jos, S. Pichardo, M. Puerto, E. Sánchez, A. Grilo, A.M. Cameán, Toxicology in Vitro Cytotoxicity of carboxylic acid functionalized single wall carbon nanotubes on the human intestinal cell line Caco-2, Toxicology in Vitro. 23 (2009) 1491–1496.

[35] K.K. Bansal, D. Kakde, U. Gupta, N.K. Jain, Development and characterization of triazine based dendrimers for delivery of antitumor agent, Journal of Nanoscience and Nanotechnology. 10 (2010) 8395–8404.

[36] K. Mori, Y. Sasaki, S. Sai, S. Kaneda, H. Hirahara, Y. Oishi, et al., Electrochemical polymerization of 2-(dioctylamino)-1, 3, 5-triazine-4, 6-dithiol on iron plates, Langmuir. 11 (1995) 1431–1434.

[37] J. Zhu, B. Deng, J. Yang, D. Gang, Modifying activated carbon with hybrid ligands for enhancing aqueous mercury removal, Carbon. 47 (2009) 2014–2025.

[38] L. Minati, G. Speranza, S. Torrengo, L. Toniutti, C. Migliaresi, D. Maniglio, et al., Characterization of thiol-functionalized carbon nanotubes on gold surfaces, Surface Science. 604 (2010) 1414–1419.

[39] F. Wang, Y. Wang, Y. Li, Preparation of 6-Diallylamino-1, 3, 5-Triazine-2, 4-Dithiol Functional Nanofilm by Electrochemical Polymerization Technique on Aluminum Surface, Int. J. Electrochem. Sci. 6 (2011) 793–803.

[40] B.A. Kakade, V.K. Pillai, An efficient route towards the covalent functionalization of single walled carbon nanotubes, Applied Surface Science. 254 (2008) 4936–4943.

[41] Y.Y.-S. Kim, J.J.-H. Cho, S.G. Ansari, H.-I.H. Kim, M.A. Dar, H.-K. Seo, et al., Immobilization of avidin on the functionalized carbon nanotubes, Synthetic Metals. 156 (2006) 938–943.

[42] Y. Wang, Z. Iqbal, S. V Malhotra, Functionalization of carbon nanotubes with amines and enzymes, Chemical Physics Letters. 402 (2005) 96–101.

[43] M.C. Dujardin, C. Caze, I. Vroman, Ion-exchange resins bearing thiol groups to remove mercury.: Part 1: synthesis and use of polymers prepared from thioester supported resin, Reactive and Functional Polymers. 43 (2000) 123–132.

[44] L. Blue, P. Jana, D. Atwood, Aqueous mercury precipitation with the synthetic dithiolate, BDTH 2, Fuel. 89 (2010) 1326–1330.

[45] A. Hutchison, D. Atwood, Q.E. Santilliann-jiminez, The removal of mercury from water by open chain ligands containing multiple sulfurs, Journal of Hazardous Materials. 156 (2008) 458–465.

[46] K. Pillay, E.M. Cukrowska, N.J. Coville, Improved uptake of mercury by sulphur-containing carbon nanotubes, Microchemical Journal. 108 (2013) 124–130.

[47] M. Sánchez-Polo, J. Rivera-Utrilla, Adsorbent-adsorbate interactions in the adsorption of Cd(II) and Hg(II) on ozonized activated carbons., Environmental Science & Technology. 36 (2002) 3850–4.

[48] Y.-S.L. Cheng-Chung Liu, Ming Kuang-Wang, Removal of Nickel from Aqueous Solution Using Wine Processing Waste Sludge, Industrial & Engineering Chemistry Research. 44 (2005) 1438–1445.

[49] Y. Liu, Y.-J. Liu, Biosorption isotherms, kinetics and thermodynamics, Separation and Purification Technology. 61 (2008) 229–242.

[50] G. Rao, C. Lu, F. Su, Sorption of divalent metal ions from aqueous solution by carbon nanotubes: A review, Separation and Purification Technology. 58 (2007) 224–231.

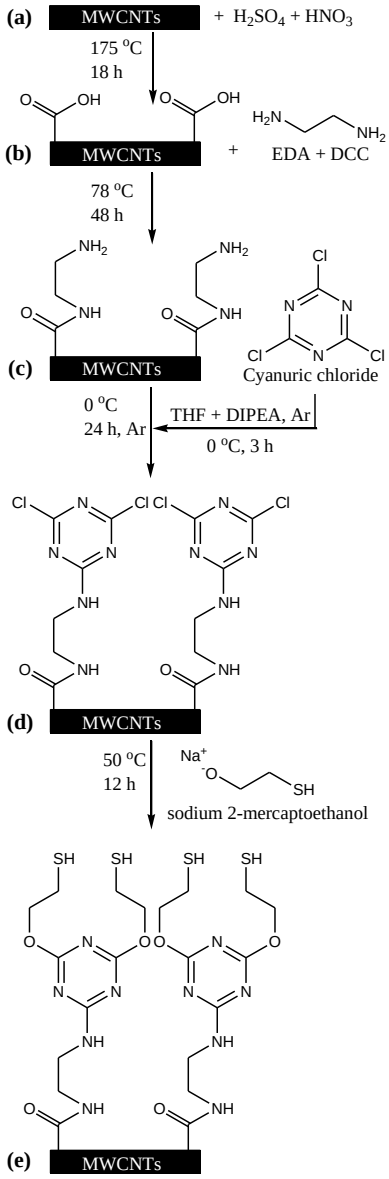

Fig. 1. Schematic of the functionalization of the MWCNTs.

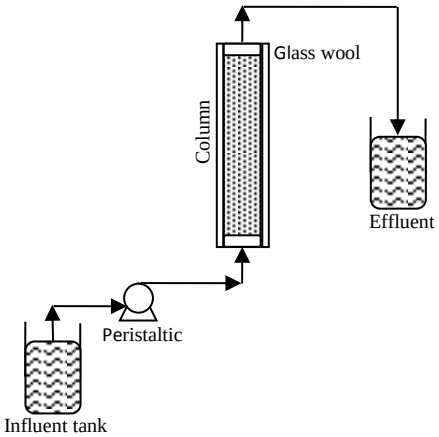

Fig. 2. Schematic diagram for the fixed-bed glass column.

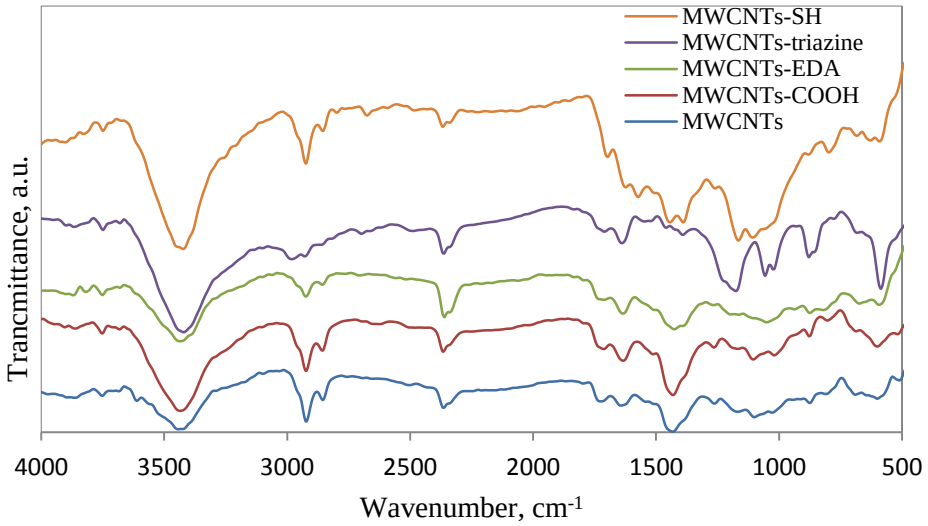

(a)

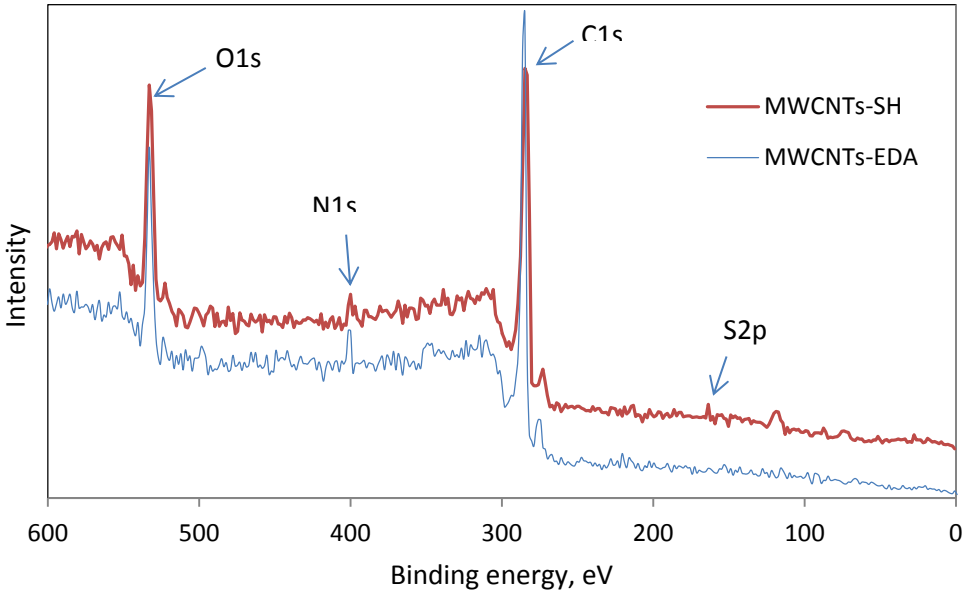

(b)

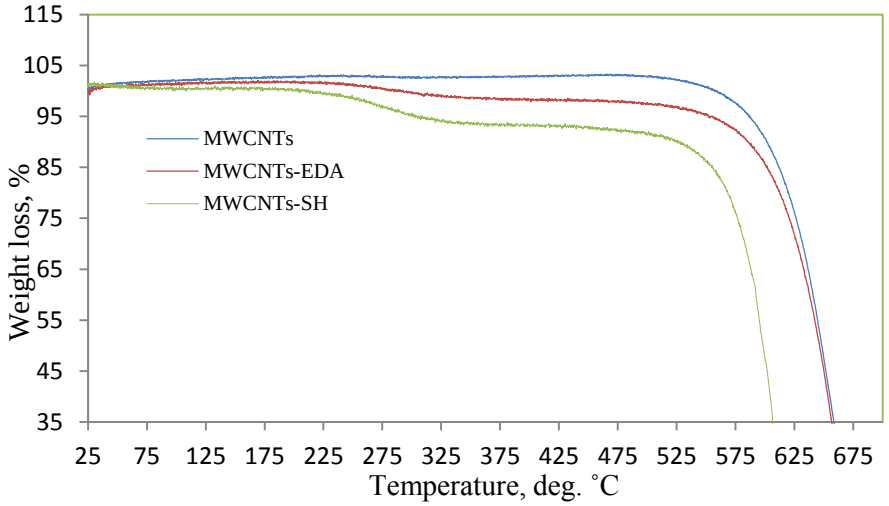

(c)

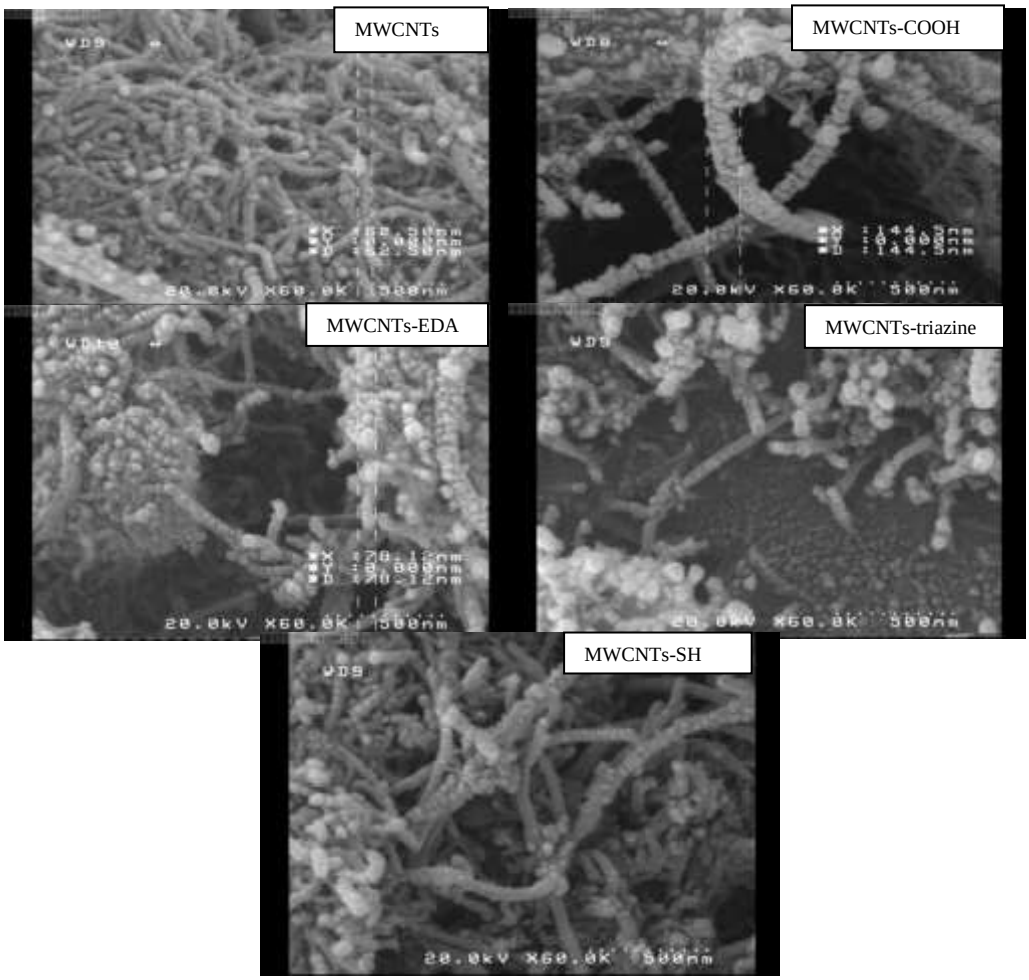

(d)

Fig. 3. Characteristics of functionalized MWCNTs (a) FT-IR spectra of pristine and functionalized MWCMTs, (b) XPS spectra of wide scan of the MWCNTs-EDA and MWCNTs-SH, (c) TGA curves and (d) scanning electron microscope.

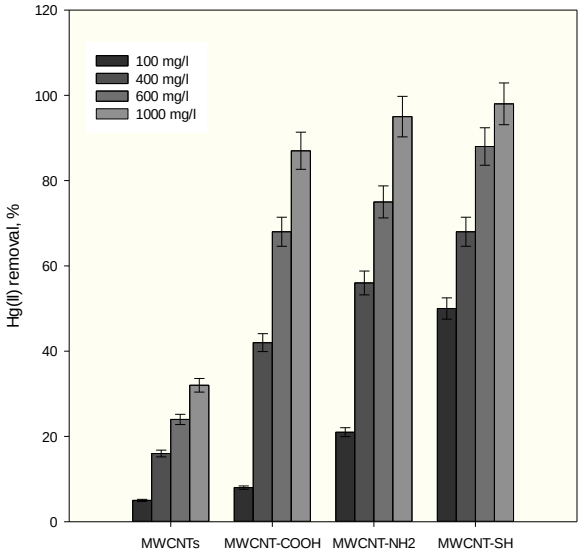

Fig. 4. Effect of adsorbent dose on the Hg(II) removal by pristine and functionalized MWCNTs. Conditions: initial Hg(II) concentration 10 mg/l, initial pH value 7, agitation time 60 min at 200 rpm and 25 ˚C.

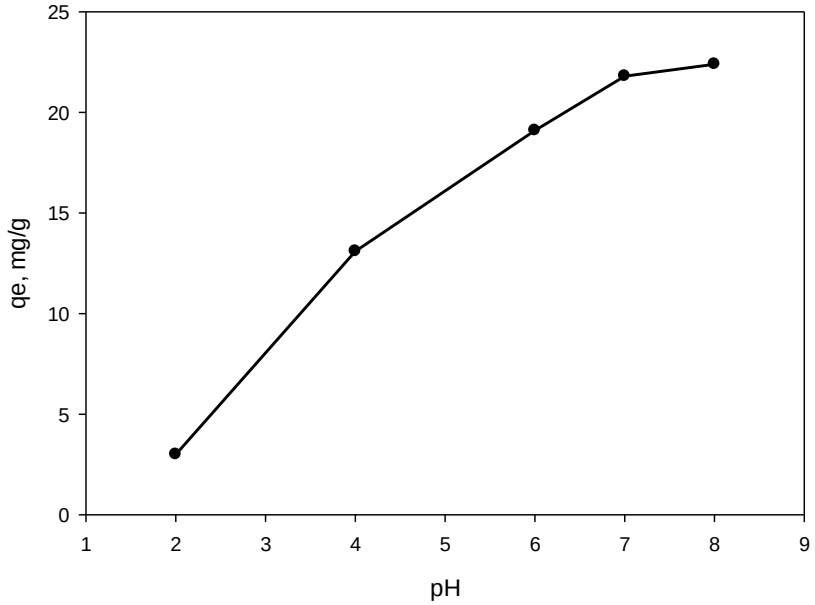

Fig 5. Effect of pH on Hg(II) removal. Conditions: adsorbent dose 400 mg/l, initial concentration 10 mg/l, agitation time 60 min in 200 rpm and at 25 ˚C.

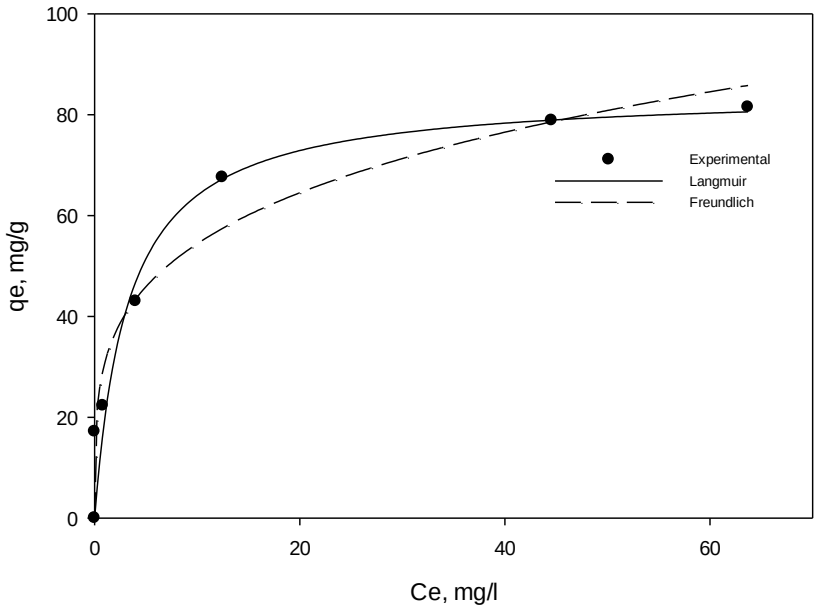

Fig. 6. Adsorption isotherm of Hg(II) on MWCNT-SH at initial metal ions concentration from 5–100 mg/l, adsorbent dose of 400 mg/l, pH 6.0 and temperature of 25 ˚C for 60 min.

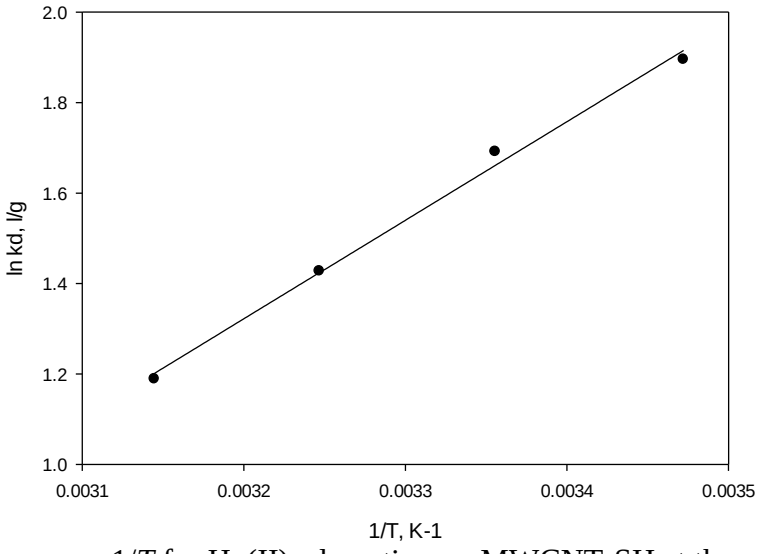

Fig. 7. Plots of ln k_d versus 1/T for Hg(II) adsorption on MWCNT-SH at the adsorbent dose of 400 mg/l, pH 6.0 and different temperatures.

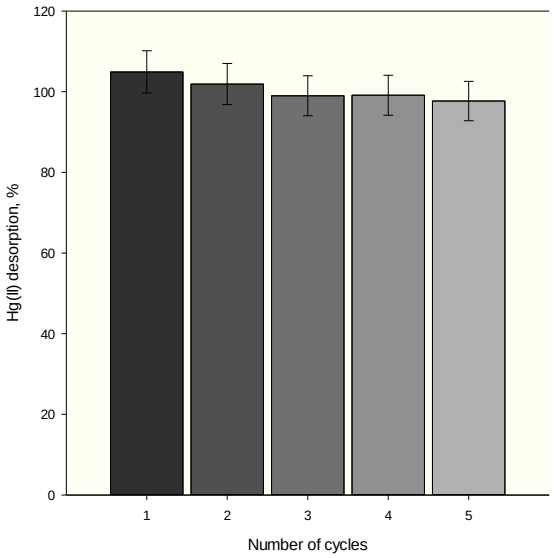

Fig. 8. The number of adsorption-desorption cycle of Hg(II) on MWCNT-SH.

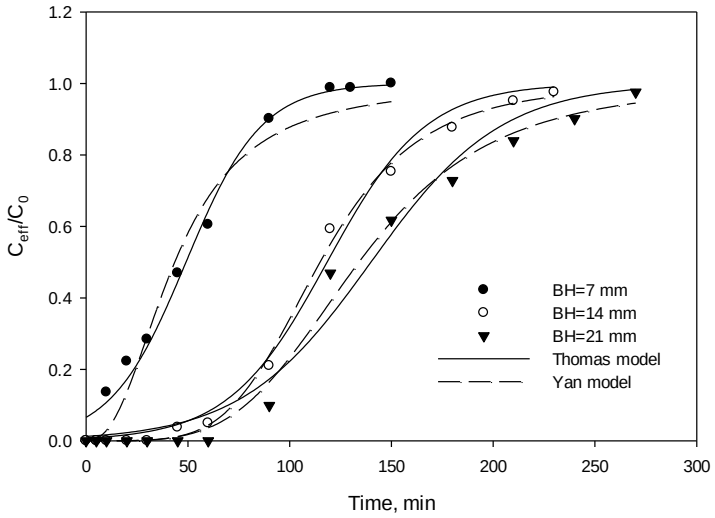

(a)

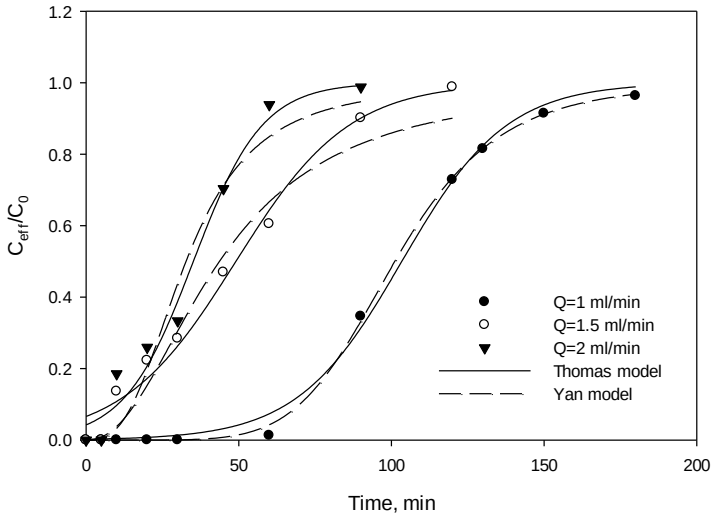

(b)

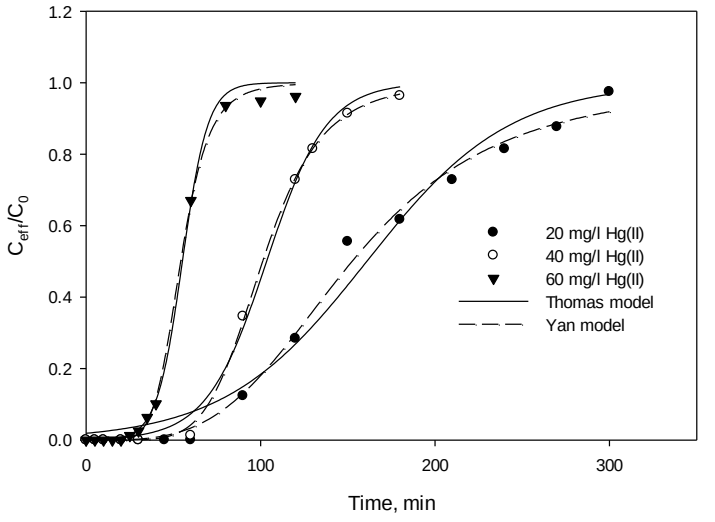

(c)

Fig. 9. Experimental (symbols) and theoretical (solid and dotted lines) breakthrough curves in (a) different bed heights, (b) different flow rates and (c) different influent ion concentration for Hg(II) removal by the MWCNT-SH.

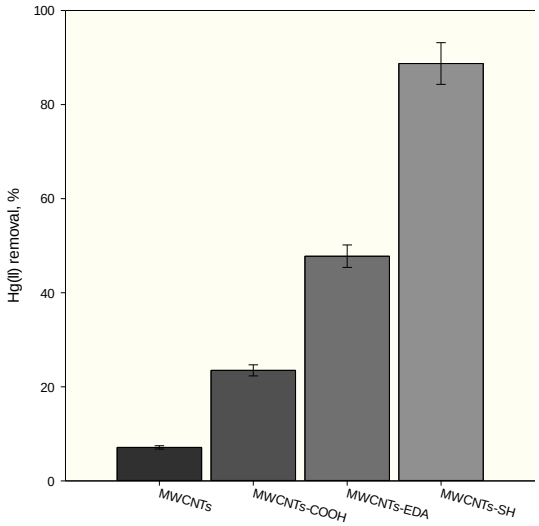

Fig. 10. Removal of Hg ions from chloralkali wastewater with different adsorbents. Adsorbent dose 200 mg/l, pH=6 and room temperature.

Table 1. Langmuir and Freundlich parameters for adsorption of Hg(II) onto MWCNT-SH

Langmuir			Freundlich		
q_m *(mg/g)*	*b (l/mg)*	R^2	*n*	k_f	R^2
84.66	0.31	0.945	0.301	30.924	0.926

Table 2. Thermodynamic parameters of Hg(II) adsorption on MWCNT-SH at different temperatures in Kelvin (initial concentration of metal ion 40 mg/l).

ΔH° (kJ mol^{-1})	ΔS° ($kJ^{-1}mol^{-1}K^{-1}$)	ΔG° (kJ mol^{-1})				R^2
		288 K	298 K	308 K	318 K	
-18.12	-0.047	-4.59	-4.12	-3.65	-3.18	0.995

Table 3. Kinetic adsorption parameters obtained using pseudo-first-order and pseudo-second-order models

Metal conc. (mg/l)	q_e^{exp} (mg/g)	Pseudo-first-order			Pseudo-second-order		
		k_1 (min^{-1})	q_{e1} (mg/g)	R^2	k_2 (g/mg min)	q_{e2} (mg/g)	R^2
5	16.85	0.41	10.91	0.8720	2.05	16.94	1.0000
10	22.65	0.028	6.02	0.7680	0.02	22.73	0.9990
20	41.66	0.07	14.48	0.5820	0.027	41.66	0.9980
40	70.00	0.023	26.67	0.7810	0.0038	70.92	0.9990
80	82.07	0.018	24.1	0.5490	0.0042	81.97	0.9990
100	82.47	0.025	36.47	0.7640	0.0025	83.33	0.9990

Table 4. The breakthrough parameters and predicted values of Thomas and Yan models for Hg(II) removal at various column conditions.

Column condition[a]			Breakthrough analysis [b]				Thomas model[c]			Yan model[d]		
BH	Q	Conc.	q_e	*R*, %	C_e	MTZ	q_{Th}	$k_{Th}\times10^4$	R^2	q_Y	a	R^2
7	1	40	105.65	64.03	14.38	4.41	103.4	14.57	0.996	101.13	5.950	0.999
7	1.5	40	76.42	42.46	23.01	6.35	73.52	13.5	0.995	65.23	2.371	0.975
7	2	40	71.47	52.55	18.97	6.79	70.18	22.18	0.978	65.38	2.854	0.957
7	1	20	83.08	55.34	8.93	5.46	80.4	12.25	0.997	76.19	3.591	0.994
7	1	60	86.28	69.30	18.61	4.13	82.71	22.88	0.982	81.223	6.644	0.999
14	1.5	40	91.37	57.19	17.12	9.9	88.74	10.32	0.994	86.16	4.717	0.998
21	1.5	40	72.86	53.97	18.41	16.02	69.94	7.83	0.980	66.98	4.074	0.993

[a] BH: bed height (mm); Q: flow rate (ml/min); Conc.: influent metal ion concentration (mg/l).
[b] q_e: adsorption capacity (mg/g); R%: removal percentage; C_e: equilibrium concentration (mg/l); MTZ: mass transfer zone (mm).
[c] k_{Th}: Thomas rate constant (ml/min/mg); q_{Th}: Thomas maximum adsorption capacity (mg/g).
[d] a: Yan rate constant (dimensionless); q_Y: Yan maximum adsorption capacity (mg/g).

Table 5. Characteristics of chloralkali wastewater

Characteristics	Values
pH	6
TS	24 g/l
TVS	325 mg/l
EC	43.5 mS/cm
Cl^-	12800 mg/l
Na^+	9300 mg/l
K^+	38 mg/l
Mg^{+2}	40 mg/l
Zn^{+2}	10 mg/l
Fe^{+2}	1.2 mg/l
Mn^{+2}	0.03 mg/l
Hg^{+2}	64.7 µg/l